

Morphologies of monoclinic phase in ZrO_2 (2 mol% Y_2O_3) revealed by TEM *in situ* continuous observations

T. C. LEI, G. Y. LIN, Q. L. GE, Y. ZHOU, X. J. HE

Department of Metals and Technology, Harbin Institute of Technology, Harbin 150001, People's Republic of China

TEM *in situ* continuous observations were made of the tetragonal (t) to monoclinic (m) transformation of $\text{ZrO}_2(2\text{Y})$ in pure $\text{ZrO}_2(2\text{Y})$ and $\text{Al}_2\text{O}_3 + 25 \text{ vol } \% \text{ZrO}_2(2\text{Y})$ ceramics. It was found that there were two morphologies of the m-phase after transformation of the t-grains: N-shaped plate clusters and parallel laths. The parallel lath morphology is considered to be the result of lateral growth of the m-plates. The lower the local Y_2O_3 content, the less will be the stability of the t-phase, and then the larger will be the possibility of the lateral growth of the m-plates. This, in turn, facilitates the transition from N-shaped to parallel lath morphology and increases the completeness of the transformation.

1. Introduction

The t–m transformation of ZrO_2 has been widely studied and recognized as one of the most important toughening factors used in ceramics [1–5]. Although some TEM *in situ* observations of this transformation have been made [6–14], detailed investigations concerning the microstructural changes (including nucleation and growth, as well as the morphology of the martensitic (m) phase) have seldom been reported. Therefore, in comparison with the long-term accumulation of knowledge of the martensitic and bainitic transformations in steels and alloys, ceramic materials with phase-transformable ZrO_2 cannot be exactly controlled in order to obtain predicted microstructure with pre-designed properties. Therefore, much attention needs to be paid to the careful study of the microstructural changes of ZrO_2 -containing ceramics in order to develop further its toughening effect. In this study TEM *in situ* continuous observations of the tetragonal to martensitic (t–m) transformations were made on $\text{ZrO}_2(\text{Y}_2\text{O}_3)$ and $\text{ZrO}_2(\text{Y}_2\text{O}_3) + \text{Al}_2\text{O}_3$ ceramics and the detailed microstructural changes have been discussed.

2. Experimental procedure

$\text{ZrO}_2(2\text{Y})$ with 2 mol% Y_2O_3 and Al_2O_3 powders with average grain sizes of nearly 0.05 and 0.1 μm , respectively, were used as the raw materials for investigation. Pure $\text{ZrO}_2(2\text{Y})$ and $\text{Al}_2\text{O}_3 + 25 \text{ vol } \% \text{ZrO}_2(2\text{Y})$ mixtures were sintered by hot pressing at 1650 °C for 1 h under a pressure of 25 MPa. X-ray diffraction analysis showed that in the hot-pressed state, the structure of the $\text{ZrO}_2(2\text{Y})$ exhibits a mixture of t + m phases in both pure $\text{ZrO}_2(2\text{Y})$ and $\text{Al}_2\text{O}_3 + \text{ZrO}_2(2\text{Y})$ composite. Discs of 20 mm

diameter \times 5 mm were cut into thin sheets 0.3 mm thick, which were milled to nearly 30 μm thickness cut into dishes of 3 mm diameter. These milled dishes were then gripped between two pieces of copper net and glued together with resin. The well-glued specimens were thinned by using a Gaton 600 ion-thinner. The centre of the copper net was denuded leaving a copper ring which was used as a supporting skeleton to protect the thin foil against breakage. The foils were then observed in a Philips CM12 electron microscope operated at 120 kV.

The possibility of TEM *in situ* continuous observation of t–m transformation of ZrO_2 under the heating effect of the electron beam has been explained by some authors [7, 8] as the result of high local thermal stresses at the boundaries of the tetragonal grains, generated by the electron beam. However, this explanation cannot be easily accepted, because of the lack of experimental evidence and because the nature of the thermal stresses is not clear (only tensile stress is favourable to the t–m transformation). In a previous work [12] we have shown by thermal expansion analysis that at a heating rate of 60 °C min⁻¹ only the reverse m–t transformation occurs in the temperature range 450–550 °C upon heating. However, at a much lower heating rate of 10 °C min⁻¹, besides the m–t transformation, the t–m transformation at 100–300 °C can also be found. Because the t–m transformation is time-dependent [2, 3, 12], high heating rates will cause the specimens to pass quickly through the low-temperature range for t–m transformation, and directly into the higher temperature range for normal m–t transformation. The slow rate of heating and a lower temperature range can just be obtained when observing thin foils in the electron microscope (with no special heating stand). In this case the occurrence of

the t–m transformation in a material having t + m phases may be considered as the result of the removal of residual internal stresses accumulated by volumetric expansion during the t–m transformation upon cooling from the sintering temperature. Certainly, it is worth noting that the specific features of the t–m transformation observed on thin foils in an electron microscope, may differ to some extent from those in bulk material under normal circumstances, but in any case the information obtained by *in situ* observations using TEM will be interesting and useful for a good understanding of the details of microstructural changes.

3. Results and discussion

A set of transmission electron micrographs of *in situ* continuous observations of the t–m transformation in pure $\text{ZrO}_2(2\text{Y})$ is shown in Fig. 1. It can be seen that the plates of m-phase (examined by selected-area diffraction, not shown in the figure) nucleate preferentially at boundaries of t-grains, pass across the grains to the opposite side and induce there the nucleation of new plates by an autocatalytic effect (Fig. 1a, b). Sometimes the plates grow partway across the grain and stop at some barriers (Fig. 1b), and some of the plates can grow through the boundary into the adjacent grain with only a slight inclination of direction (Fig. 1b, c left). With increasing the time of exposure to the electron beam, the number of plates increases, forming a N-shaped morphology of the plate clusters (Fig. 1d, e, f) very similar to the morphology of martensite structure in high-carbon steels. In the meantime, it can be seen clearly that in addition to an increase in the number of plates, their width also increases with time (see Fig. 1b, c, d). By measuring the width changes of plates with time, an average rate of widening of the plates has been estimated to be nearly 0.5 nm s^{-1} (over the range $0.3\text{--}0.8 \text{ nm s}^{-1}$). The longitudinal growth rate of the plates is too large to be measured. Once the plates have nucleated, their longitudinal growth is almost completed, very like the martensitic plates in steels. In general, the t–m transformation of ZrO_2 is considered to be martensitic because of the displacive character of the transformation, as well as other specific features such as the large volumetric effect, orientational relationships, habit plane, surface relief, etc. Recently, this transformation has been considered as bainite-like [14] on the basis of thermal expansion measurements. Following the results of *in situ* observations given in Fig. 1, it can be concluded that during the t–m transformation, the martensitic type of nucleation with very fast longitudinal growth of the plates of m-phase, is accompanied by a slower rate of lateral growth of the plates. The increase in the volume fraction of m-phase with time may be considered as the result of the addition of the increased number of plates and their lateral growth, i.e. a martensitic nucleation plus a bainitic lateral growth of the m-plates.

Another set of transmission electron micrographs of pure $\text{ZrO}_2(2\text{Y})$ is shown in Fig. 2. The m-phase plates initially nucleate as N-shaped clusters (Fig. 2a–c) but

the morphology gradually changes to parallel laths (Fig. 2d–f), like lath martensite in low-carbon steels. This morphological transition occurs mainly by a strongly developed lateral growth of the plates. Transmission electron micrographs of the *in situ* TEM observations of the t–m transformations of t- $\text{ZrO}_2(2\text{Y})$ grains in the $\text{Al}_2\text{O}_3 + 25 \text{ vol } \% \text{ ZrO}_2(2\text{Y})$ composite shown in Fig. 3 indicate more clearly the transition of N-shaped plate clusters to parallel lath morphology of the m-phase. Four m-plates nucleate and grow very quickly in the longitudinal direction (Fig. 3a) forming an N-shaped morphology. Then the plates grow laterally at a much lower rate and the number of plates is not increased, so that the transformation proceeds primarily by lateral growth of the plates nucleated in the first stages of transformation. Comparing the two distinct morphologies given in Fig. 1 and Figs 2, 3, it can be concluded that the N-shaped morphology is always the initial morphology of the m-phase obtained in the first stages of transformation. If the lateral growth of the m-plates is possible (as shown in Figs 2 and 3) the transformation will continue to proceed and the transition of N-shaped morphology will take place so that a final parallel lath morphology will appear. If the lateral growth of the m-plates is impossible, as in the case of Fig. 1, the N-shaped morphology will be the final form and the transformation cannot continue and is incomplete. In addition, it can be seen from Fig. 1f that the N-shaped morphology is accompanied by the incompleteness of transformation. In micro-areas among the plates, the t-phase remains untransformed owing to the constraints of compressive stresses accumulated by large (nearly 5%) volumetric expansion during the t–m transformation. However, in parallel lath morphology shown in Figs 2f and 3d, the micro-areas between the m-plates are filled by the lateral growth of the plates, so that almost the entire grain of the t-phase underwent the t–m transformation. Thus, the incompleteness of transformation due to the sluggish lateral growth of the m-plates is also a specific feature of the N-shaped morphology in comparison with the parallel lath one. Therefore, the possibility of the sidewise growth of the m-plates will be a controlling factor in determining the final morphology and completeness of the t–m transformation of $\text{ZrO}_2(2\text{Y})$ ceramics.

In general, the martensitic t–m transformation of ZrO_2 may be divided into two steps as described earlier [11]. The first step is the reformation of the lattice structure from tetragonal to monoclinic by means of shearing displacement of zirconium ions, and the second step is the diffusional migration of oxygen ions to their proper positions in the monoclinic lattice. It may be thought that the rapid shear displacement of zirconium ions will be the leading factor for nucleation and longitudinal growth of the m-plates, while the diffusional migration of oxygen ions will be the leading factor for slow lateral growth of the plates. The possibility and degree of development of the lateral growth depend primarily upon the stability of the t-phase of ZrO_2 , and the stability of the t-phase is determined by the Y_2O_3 content of ZrO_2 .

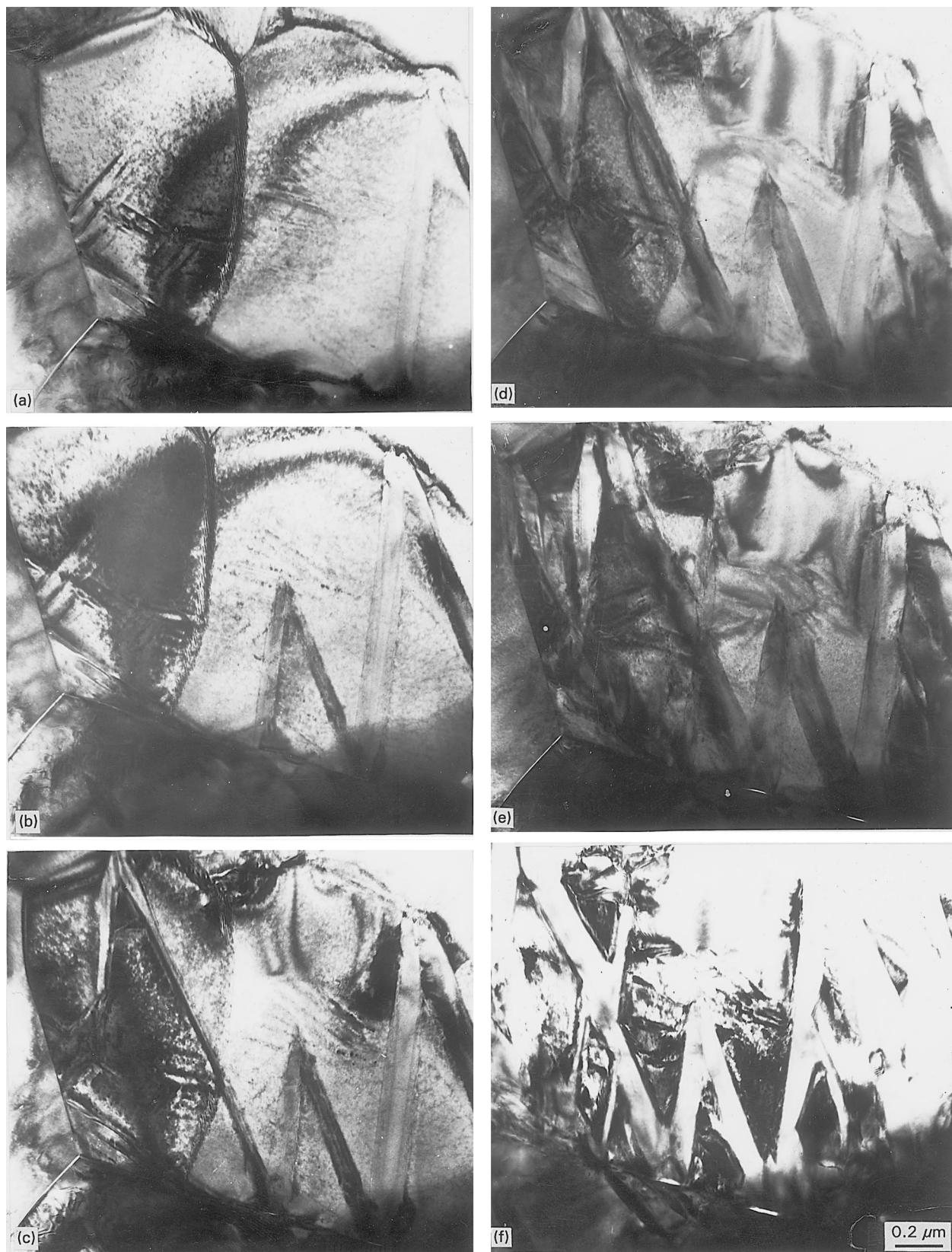


Figure 1 A series of transmission electron micrographs of ZrO_2 (2Y) ceramics showing nucleation and growth of m-plates in prior t-grains with various times of exposure to an electron beam after taking the first photograph: (a) $t = 0$ s; (b) $t = 10$ s; (c) $t = 60$ s; (d) $t = 140$ s; (e) $t = 350$ s; (f) $t = 1200$ s and after tilting at an angle.

Fig. 4 shows the local Y_2O_3 contents in various sites of the grains after the t-m transformation. In this study, the nominal content of Y_2O_3 is 2 mol %, but the distribution of Y_2O_3 content is not uniform. The N-shaped morphology is accompanied by a higher Y_2O_3 content of the prior t-grain (Fig. 4a) while the

parallel lath morphology is accompanied by a lower Y_2O_3 content (Fig. 4b). The nucleation of the m-plates occurs on grain boundaries where the Y_2O_3 is low (Fig. 5) and ceases where the Y_2O_3 is high. The high Y_2O_3 content and the compressive stress accumulated in front of the m-plates may act as barriers preventing

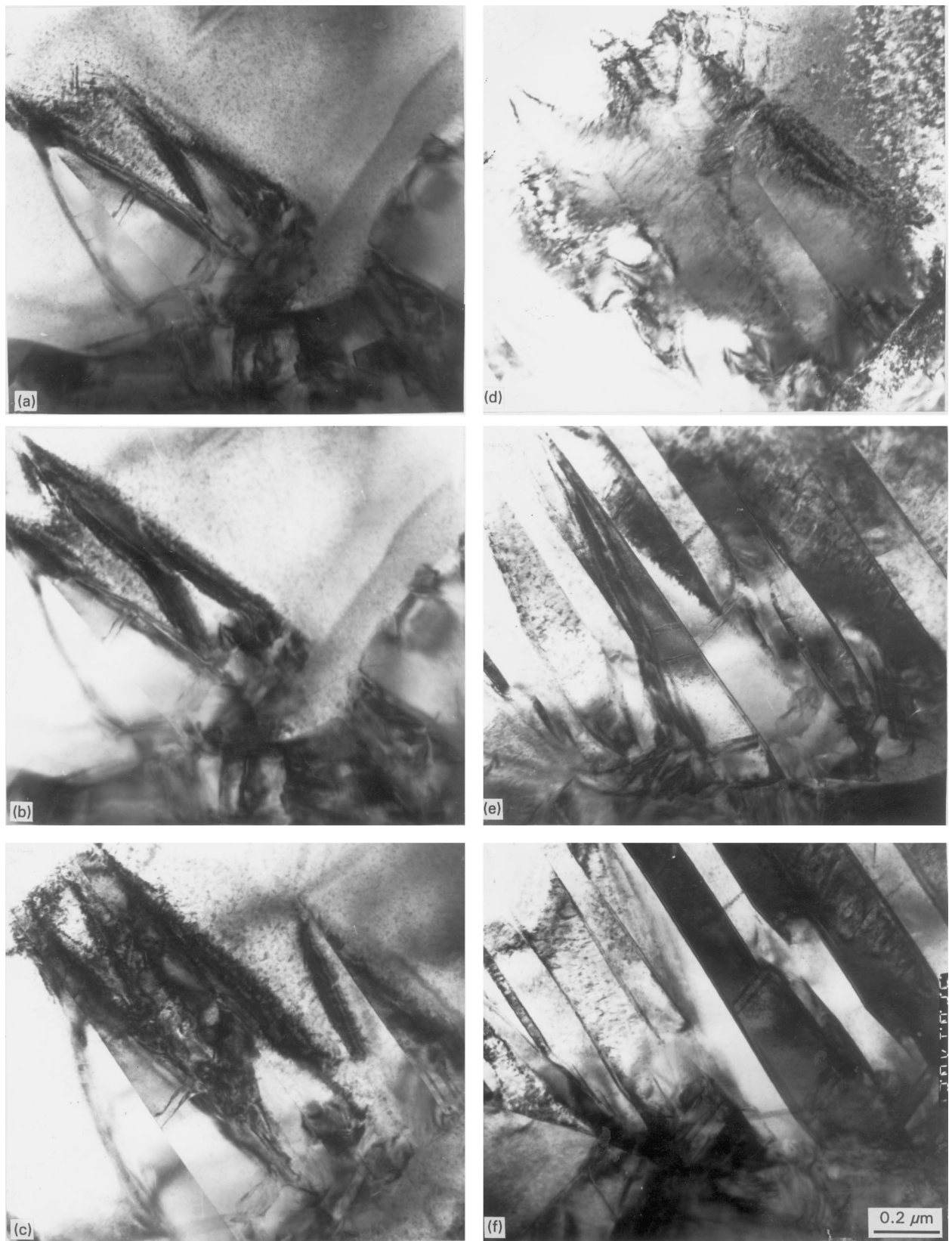


Figure 2 Another series of transmission electron micrographs of $\text{ZrO}_2(2\text{Y})$ ceramics showing the nucleation and growth of m-plates in prior t-grains with various times of exposure to an electron beam after taking the first photograph: (a) $t = 0$ s; (b) $t = 15$ s; (c) $t = 50$ s; (d) $t = 110$ s; (e) $t = 200$ s; (f) $t = 300$ s.

the plates from their longitudinal growth, straight to the opposite side of the t-grains, and causing the latter to stop partway, as shown in Figs 1b and 5.

Therefore, the local distribution of Y_2O_3 content is the most important factor in determining the morpho-

logy of the m-phase in the t-m transformation of $\text{ZrO}_2(2\text{Y})$ ceramics. The higher the Y_2O_3 content, the higher will be the stability of the t-phase and the larger will be the resistance to t-m transformation. A lower Y_2O_3 content is always favourable to a larger number of

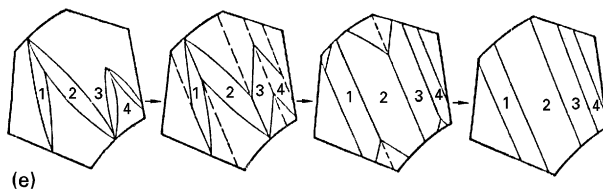
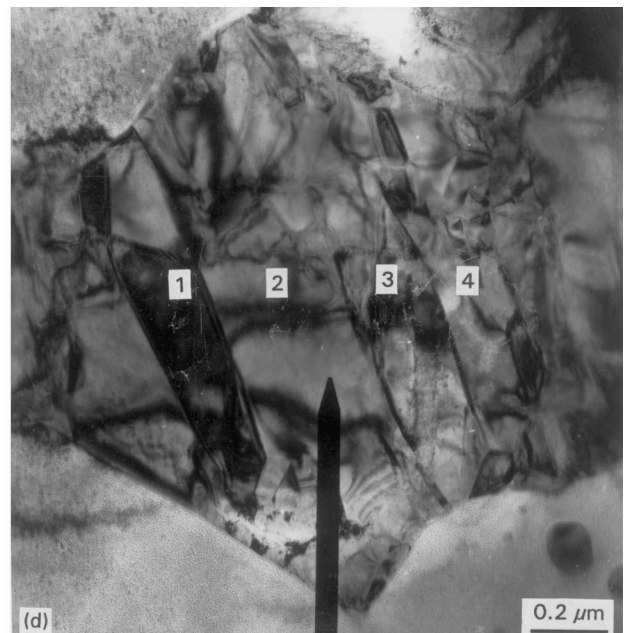
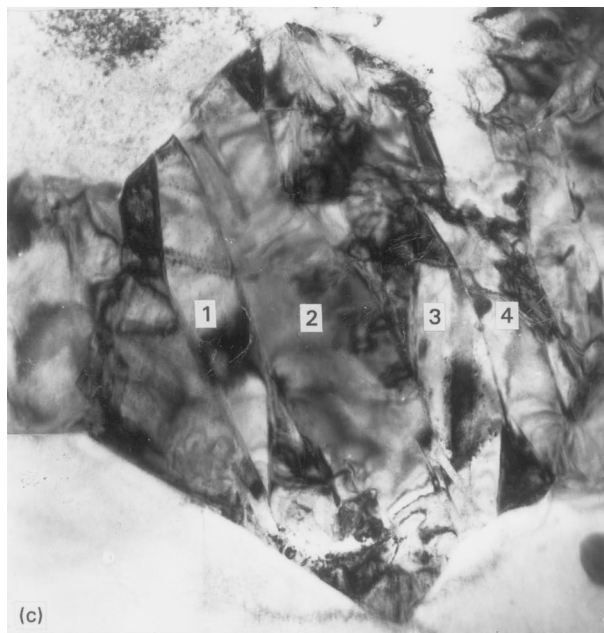
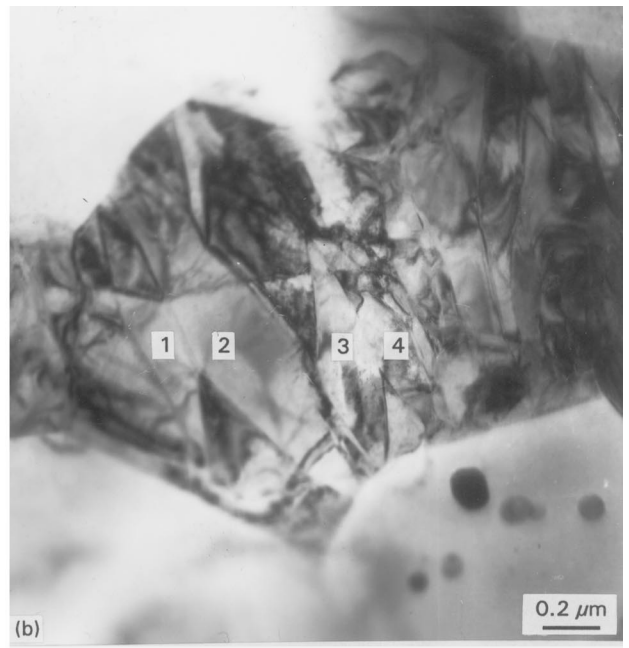
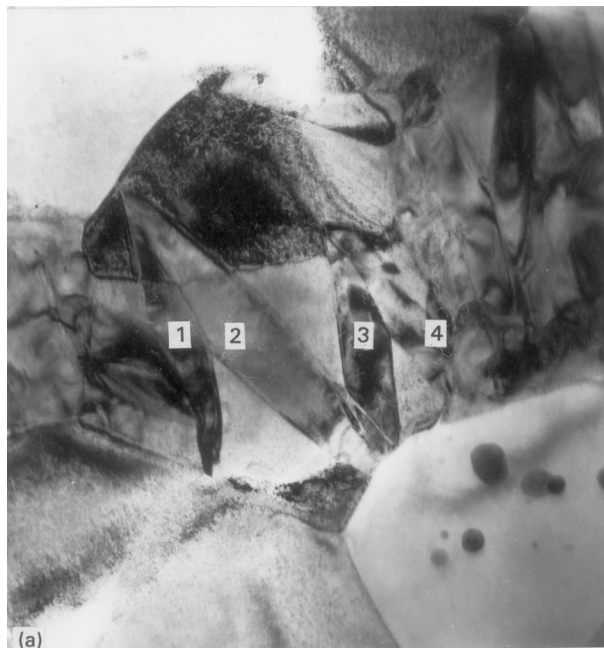


Figure 3 A series of transmission electron micrographs of $\text{Al}_2\text{O}_3 + 25 \text{ vol } \% \text{ ZrO}_2(2\text{Y})$ composite showing the nucleation and growth of m-plates in a prior t-grain with various times of exposure to an electron beam after taking the first photograph: (a) $t = 0 \text{ s}$; (b) $t = 30 \text{ s}$; (c) $t = 120 \text{ s}$; (d) 270 s ; (e) schematic representation showing the lateral growth of the m-plates and the transition from N-shaped morphology to parallel laths.

nucleation sites and easier longitudinal growth of the m-plates across the t-grains, and also to easier lateral growth of the plates and thus to a more complete transformation and the appearance of parallel lath morphology.

Fig. 6 shows a series of *in situ* transmission electron micrographs indicating the t-m transformation in a t-grain of the $\text{Al}_2\text{O}_3 + 25 \text{ vol } \% \text{ ZrO}_2(2\text{Y})$ composite after longer exposure times to the electron beam in comparison with the photographs shown in Fig. 3. Here, with the progress of t-m transformation presented by the nucleation of m-plates with time,

a gradual reduction of a pre-existing m-plate (in the lower right part of the grain) can be seen, indicating that the m-t transformation occurs together with the t-m transformation in one grain. The reduction of the m-plate in a t-grain has been observed by McCartney and Rühle [10] by increasing the beam intensity. However, in this study, it was observed after prolonged exposure of the specimen to the electron beam. These two conditions may be considered identical, because they both offer a much higher heating temperature at which the inverse m-t transformation regularly occurs. The rate of the decrease in length of the

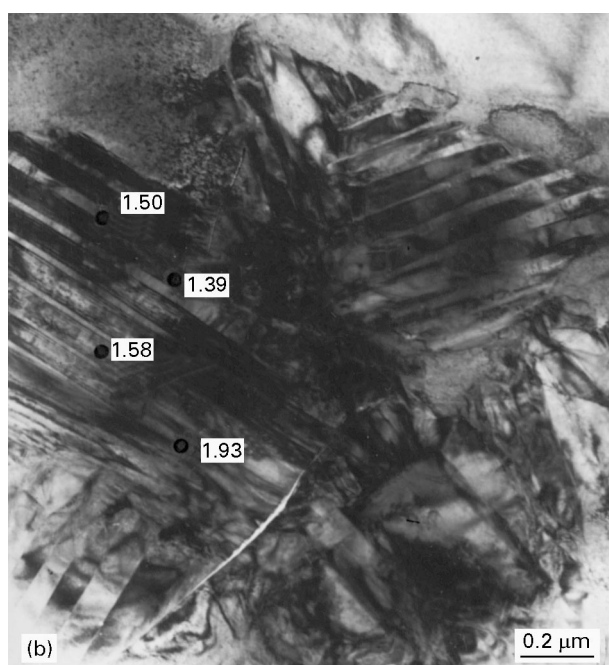
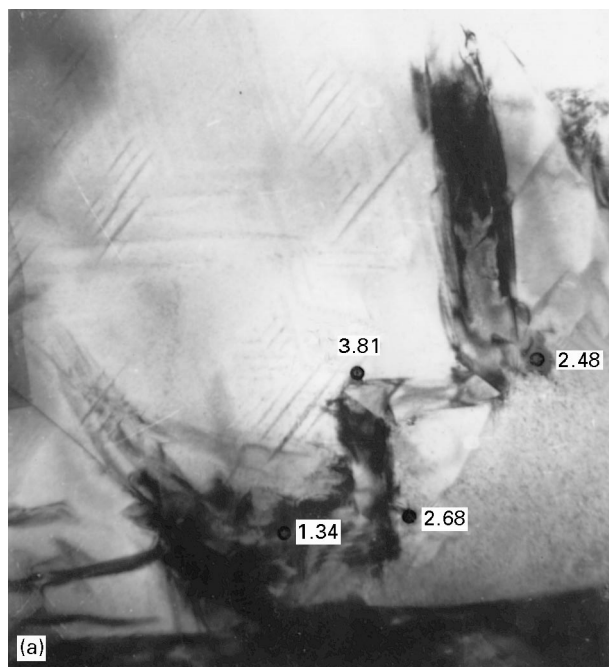


Figure 4 Local distribution of the Y_2O_3 content (mol%) in prior t-grains of $ZrO_2(2Y)$ ceramics having various morphologies of the m-phase revealed by EPMA: (a) N-shaped morphology; (b) parallel lath morphology.

diminishing m-plate has been measured to be nearly 0.5 nm s^{-1} , which is the same as the rate of lateral growth of the m-plate during t-m transformation, as mentioned above. Therefore, it can be concluded that the reverse m-t transformation is a diffusion-controlled process having a measurable low rate. The reformation of the lattice structure from monoclinic to tetragonal and the migration of zirconium and oxygen ions to their proper positions, are controlled by diffusional displacements of these ions.

4. Conclusions

1. TEM *in situ* continuous observations indicate that during the t-m transformation of $ZrO_2(2Y)$ in

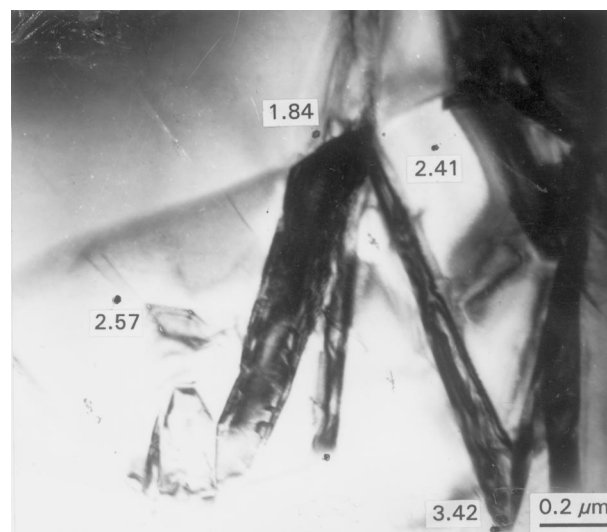


Figure 5 Local distribution of the Y_2O_3 content (mol%) in a $ZrO_2(2Y)$ grain of the $Al_2O_3 + 25 \text{ vol} \% ZrO_2(2Y)$ composite revealed by EPMA.

pure $ZrO_2(2Y)$ or $Al_2O_3 + ZrO_2(2Y)$ ceramics m-plates nucleate preferentially at boundaries of t-grains in an autocatalytic manner, with the number of plates increasing with time. In the first stages of transformation, the m-plates are arranged in forms of N-shaped clusters.

2. The fast nucleation and longitudinal growth of the m-plates is accompanied by a slow lateral growth of the plates. Nucleation and longitudinal growth of the plates is mainly attributed to the shear displacement of zirconium ions to reform the lattice from tetragonal to monoclinic structure, while the lateral growth is related to the diffusive migration of the oxygen ions to their proper positions in the m-lattices.

3. Two different morphologies of the arrangement of m-plates can be found: N-shaped clusters and parallel laths, depending on the possibility of lateral growth of the m-plates. N-shaped clusters of the m-plates are accompanied by an incomplete transformation with the intercluster micro-areas between the plates remaining in their initial t-phase state. The parallel lath morphology may be considered to be the result of well-developed lateral growth of the plates and thus is accompanied by a much larger completeness of transformation.

4. Local distribution of the Y_2O_3 content is the most important factor in determining the final morphology of the m-phase. The lower the Y_2O_3 content, the lower will be the stability of $ZrO_2(2Y)$ and thus the less will be the resistance to t-m transformation. The t-grains with lower Y_2O_3 contents will have easier nucleation and longitudinal growth (across the whole grain) of the m-plates and a higher possibility of lateral growth, which will enhance the appearance of parallel morphology and the completeness of the transformation.

5. The m-t inverse transformation is a diffusion-controlled process with a rate of plate length decrease of nearly 0.5 nm s^{-1} , which is the same as the rate of lateral growth of the m-plates during the t-m transformation.

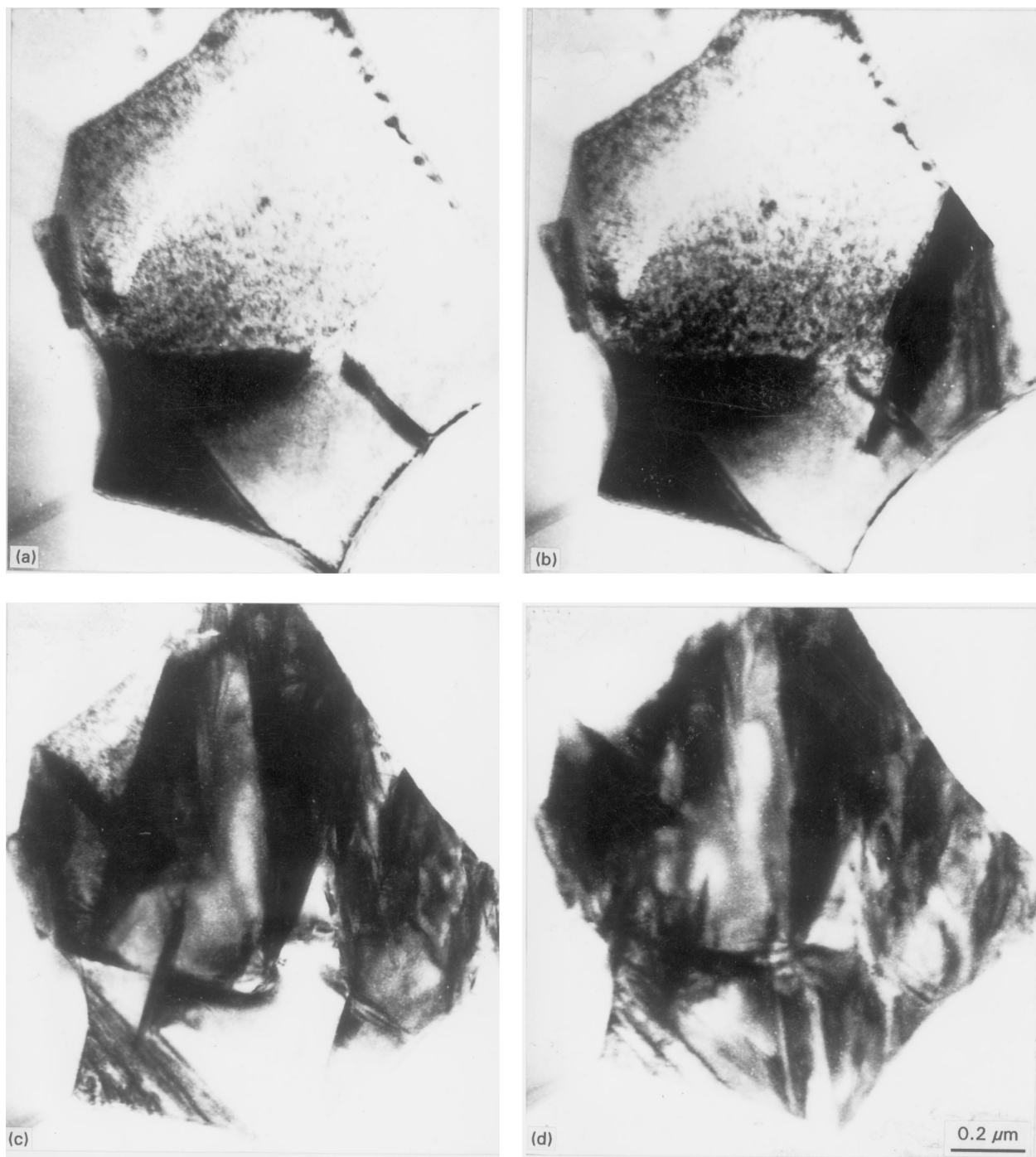


Figure 6 A series of transmission electron micrographs of $\text{Al}_2\text{O}_3 + 25 \text{ vol } \% \text{ZrO}_2(2\text{Y})$ composite showing the t-m and m-t transformations in a grain of $\text{ZrO}_2(2\text{Y})$ with various times of exposure to an electron beam after taking the first photograph: (a) $t = 360 \text{ s}$; (b) $t = 420 \text{ s}$; (c) $t = 480 \text{ s}$; (d) $t = 720 \text{ s}$.

References

1. G. K. BANSAL and A. H. HEUER, *Acta Metall.* **20** (1972) 1281.
2. N. NAKAYASHI, T. SHIGEMATSU, T. SUGIURA and H. OKINAKA, *J. Jpn Soc. Powder Technol.* **33** (1986) 356.
3. H. TSUBAKINO, R. NOZATO and M. HAMAMOTO, *J. Am. Ceram. Soc.* **74** (1991) 440.
4. J. E. BAILEY, *Proc. R. Soc. A* **279** (1964) 395.
5. N. CLAUSSEN, in "Advances in ceramics", Vol. 12: "Science and technology II", edited by N. Claussen, M. Rhule and A. H. Heuer (American Ceramic Society, Columbus, OH, 1984) p. 325.
6. M. RÜHLE, A. STECKER, D. WAIDELICH and B. KRAUS, *ibid.* p. 256.
7. A. H. HEUER and M. RÜHLE, *Acta Metall.* **33** (1985) 2101.
8. S. WEN, L. MA, J. GUO and T. YEN, *J. Am. Ceram. Soc.* **69** (1986) 570.
9. R. N. LEE and A. H. HEUER, *ibid.* **71** (1988) 701.
10. M. L. MECARTNEY and M. RÜHLE, *Acta Metall.* **37** (1989) 1859.
11. Q. L. GE, T. C. LEI, J. F. MAO and Y. ZHOU, *J. Mater. Sci. Lett.* **12** (1993) 819.
12. W. Z. ZHU, T. C. LEI and Y. ZHOU, *J. Mat. Sci.* **28** (1993) 6479.
13. Z. R. DAI, B. C. LI, H. Z. WU, Y. R. CHEN and W. X. LIU, *Acta Metall. Sinica* **27** (1991) A246.
14. N. NAKANISHI and T. SHIGEMATSU, *Mater. Trans. JIM* **32** (1991) 778.

Received 10 March 1994
and accepted 13 February 1996